Human cochlear nucleus on 7 tesla diffusion tensor imaging: insights into micro-anatomy and function for auditory brainstem implant surgery

Epprecht, Lorenz ; Qureshi, Ahad ; Kozin, Elliott D ; Vachicouras, Nicolas ; Huber, Alexander M ; Kikinis, Ron ; Makris, Nikos ; Brown, M Christian ; Reinshagen, Katherine L ; Lee, Daniel J

Abstract: OBJECTIVE: The cochlear nucleus (CN) is the target of the auditory brainstem implant (ABI). Most ABI candidates have Neurofibromatosis Type 2 (NF2) and distorted brainstem anatomy from bilateral vestibular schwannomas. The CN is difficult to characterize as routine structural MRI does not resolve detailed anatomy. We hypothesize that diffusion tensor imaging (DTI) enables both in vivo localization and quantitative measurements of CN morphology. STUDY DESIGN: We analyzed 7 Tesla (T) DTI images of 100 subjects (200 CN) and relevant anatomic structures using an MRI brainstem atlas with submillimetric (50 m) resolution. SETTING: Tertiary referral center. PATIENTS: Young healthy normal hearing adults. INTERVENTION: Diagnostic. MAIN OUTCOME MEASURES: Diffusion scalar measures such as fractional anisotropy (FA), mean diffusivity (MD), mode of anisotropy (Mode), principal eigenvectors of the CN, and the adjacent inferior cerebellar peduncle (ICP). RESULTS: The CN had a lamellar structure and ventral-dorsal fiber orientation and could be localized lateral to the inferior cerebellar peduncle (ICP). This fiber orientation was orthogonal to tracts of the adjacent ICP where the fibers run mainly caudal-rostrally. The CN had lower FA compared to the medial aspect of the ICP (0.44 ± 0.09 vs. 0.64 ± 0.08, $p < 0.001$). CONCLUSIONS: 7T DTI enables characterization of human CN morphology and neuronal substructure. An ABI array insertion vector directed more caudally would better correspond to the main fiber axis of CN. State-of-the-art DTI has implications for ABI preoperative planning and future image guidance-assisted placement of the electrode array.

DOI: https://doi.org/10.1097/mao.0000000000002565

Human Cochlear Nucleus on 7 Tesla Diffusion Tensor Imaging: Insights Into Micro-anatomy and Function for Auditory Brainstem Implant Surgery

*†Lorenz Epprecht, *†Ahad Qureshi, *†Elliott D. Kozin, ‡Nicolas Vachicouras, §Alexander M. Huber, ||¶Ron Kikinis, ||#Nikos Makris, *†M. Christian Brown, **Katherine L. Reinshagen, and *†Daniel J. Lee

**Eaton-Peabody Laboratories, Massachusetts Eye and Ear; †Department of Otology and Laryngology, Harvard Medical School, Boston, Massachusetts, USA; ‡Bertarelli Foundation Chair in Neuroprosthetic Technology, Laboratory for Soft, Bioelectronic Interfaces, Institute of Microengineering, Institute of Bioengineering, Centre for Neuroprosthetics, École Polytechnique Fédérale de Lausanne (EPFL), Lausanne, Switzerland; §Department of Otorhinolaryngology and Head and Neck Surgery, University Hospital of Zurich, Zurich, Switzerland; ||Surgical Planning Laboratory, Harvard Medical School, Boston, Massachusetts, USA; ¶Fraunhofer Institut for Medical Image Computing, University of Bremen, Bremen, Germany; #MGH Morphometric Analysis Center, Harvard Medical School; and **Department of Radiology, Massachusetts Eye and Ear Infirmary and Harvard Medical School, Boston, Massachusetts, USA*

Objective: The cochlear nucleus (CN) is the target of the auditory brainstem implant (ABI). Most ABI candidates have Neurofibromatosis Type 2 (NF2) and distorted brainstem anatomy from bilateral vestibular schwannomas. The CN is difficult to characterize as routine structural MRI does not resolve detailed anatomy. We hypothesize that diffusion tensor imaging (DTI) enables both in vivo localization and quantitative measurements of CN morphology.
Study Design: We analyzed 7 Tesla (T) DTI images of 100 subjects (200 CN) and relevant anatomic structures using an MRI brainstem atlas with submillimetric (50 μm) resolution.
Setting: Tertiary referral center.
Patients: Young healthy normal hearing adults.
Intervention: Diagnostic.
Main Outcome Measures: Diffusion scalar measures such as fractional anisotropy (FA), mean diffusivity (MD), mode of anisotropy (Mode), principal eigenvectors of the CN, and the adjacent inferior cerebellar peduncle (ICP).
Results: The CN had a lamellar structure and ventral-dorsal fiber orientation and could be localized lateral to the inferior cerebellar peduncle (ICP). This fiber orientation was orthogonal to tracts of the adjacent ICP where the fibers run mainly caudal-rostrally. The CN had lower FA compared to the medial aspect of the ICP (0.44 ± 0.09 vs. 0.64 ± 0.08, $p < 0.001$).
Conclusions: 7T DTI enables characterization of human CN morphology and neuronal substructure. An ABI array insertion vector directed more caudally would better correspond to the main fiber axis of CN. State-of-the-art DTI has implications for ABI preoperative planning and future image guidance-assisted placement of the electrode array. **Key Words:** Auditory brainstem implant—Cochlear nucleus—Diffusion tensor imaging—Image guidance—Preoperative planning.

Otol Neurotol **41:**xxx–xxx, 2020.

Patients with Neurofibromatosis type 2 (NF2) develop bilateral vestibular schwannomas (VS) that can influence cochlear nucleus (CN) structure and function through brainstem deformation (1,2). The CN is the target of the auditory brainstem implant (ABI), a neuroprosthesis that can be placed following tumor resection to restore hearing sensations in deaf NF2 patients. Placement of the multichannel surface ABI array occurs following posterior fossa craniotomy and in many cases after tumor resection in the same surgery. The CN is not directly visualized during the procedure and insertion of the array is into the lateral recess of the 4th ventricle. The surgical team relies on both indirect landmarks (root entry zone of the glossopharyngeal nerve and choroid plexus) and electrophysiology (electrically-evoked auditory brainstem responses [EABRs]) generated by the ABI to ensure accurate placement. Overall ABI outcomes are modest

Address correspondence and reprint requests to Daniel J. Lee, M.D., Department of Otology and Laryngology, Massachusetts Eye and Ear Infirmary, 243, Charles St, Boston, MA 02114, USA; E-mail: daniel_lee@meei.harvard.edu

Funding Sources: American Hearing Health Foundation (DJL/EDK), NIH P41 EB015902, P41 EB015898, DC 01089, and U24 CA180918 (RK), DOD NF170090 (to DJL), and NIDCD 01089 (to MCB).

The authors disclose no conflicts of interest.

DOI: 10.1097/MAO.0000000000002565

compared with cochlear implants, with most ABI users experiencing poor word recognition scores and in some cases failing to experience sound perception (2).

Anatomic descriptions of the CN have been limited to ex vivo anatomy and histology (3,4). One recent study specifically described the difficulties of ABI array placement on the small CN surface (5). In cases where brainstem anatomy is altered, as often encountered in NF2 patients with a large tumor burden, the knowledge from these ex vivo studies becomes more difficult to apply to specific patients.

Image-based surgical planning and navigation could improve ABI outcomes by enabling optimal and patient-specific multichannel array placement. Our research group was the first to correlate ABI array orientation as seen on routine postoperative computed tomography (CT) with perception (6). Preoperative magnetic resonance imaging (MRI) provides basic morphologic data on surgical access to the lateral recess of the 4th ventricle and the status of brainstem surface at the pontomedullary junction, but cannot resolve detailed anatomic features of the CN. This is because intensity values of the cochlear nucleus and the surrounding structures are not distinct enough to form sufficient contrast on regular clinically available T1- and T2-weighted images. Consequently, the human CN has so far evaded direct preoperative in vivo imaging.

An advanced MRI modality, termed diffusion tensor imaging (DTI), has the potential to overcome the challenge of in vivo imaging of the CN. DTI examines the direction of free water diffusion and therefore exposes the orientation of lamellar and fibrous tissue in which diffusion occurs mainly in one certain direction, such as in white matter or nerves (7). Today, the technique is often used for the differentiation of subcortical fibers that run in contrasting directions and are not seen on routine MRI. Previous studies have mapped portions of the human brainstem using DTI, including the vestibular and auditory system (8,9). In the standard brainstem atlas of Naidich Duvernoy, the CN was shown on DTI in a postmortem specimen (10). The CN, however, has not yet been characterized in vivo in a larger cohort.

In this study, we hypothesize that DTI enables the direct in vivo visualization of the CN by distinguishing it from surrounding structures, mainly the inferior cerebellar peduncle (ICP). The ICP forms the caudal, medial, and rostral borders of the CN.

MATERIAL AND METHODS

Study Design and Subjects

The study was initially approved by our Human Studies Committee (HSC #1020852-3). Data used in the preparation of this work were obtained from the Human Connectome Project (HCP) database (https://ida.loni.usc.edu/login.jsp). We randomly chose MRI images of 100 subjects (200 CN) from the HCP young healthy cohort from whom 7 Tesla (T) DTI images had been acquired. All subjects were between 22 and 35 years old and had undergone the NIH Toolbox audiometric testing (11). This test measures hearing thresholds at six different frequencies (0.5, 1, 2, 4, 6, and 8 kHz) via headphones. To provide a unifying score for Toolbox users, a single hearing metric is provided that is commonly used: A Pure-Tone Average (PTA). This is calculated by averaging the threshold scores at 1, 2, and 4 kHz. Scores for each ear are calculated, with the PTA from the better ear reported as the primary score (i.e., the ear with the lower PTA). Subjects with hearing loss greater than 10 dB were excluded from our analysis.

Image Acquisition Protocols

For anatomical reference of the diffusion data, a high-resolution 7T structural scan (Agilent Technologies, Santa Clara, CA) was acquired from an ex-vivo human brainstem as follows: Three-dimensional gradient echo pulse sequence (TR 50 ms, TE 10 ms, flip angle 60 degrees, FOV 80 × 55 × 45 mm, matrix 1,600 × 1,100 × 900), resulting in a 50 μm isotropic voxel size (Fig. 1) (12).

DTI from the HCP subjects were acquired in a 7T MRI MAGNETOM scanner (Siemens, Erlangen, Germany) by a multiband (2) spin-echo EPI sequence (repetition time (TR) 7,000 ms, echo time (TE) 71.2 ms), flip angle 90 degrees, field of view (FOV) 210 × 210 × 210 mm, matrix 200 × 200 × 200), resulting in an isotropic voxel size of 1.05 mm. B-values were 1000 s/mm^2 and 2000 s/mm^2 with 65 diffusion weighting directions each plus six b-0 images. The DTI session included four runs of approximately 9 min 50 seconds (two for each gradient table with ventral-to-dorsal and dorsal-to-ventral phase encoding polarities). Total diffusion acquisition time was approximately 40 minutes. Diffusion images were reconstructed according to the HCP pipeline as described in Sotiropoulos et al. in 2013, and corrected for distortion as in Andersson et al. in 2003 and 2015 (13–15). All HCP images had the same coordinate system and were rigidly registered (12 degrees of freedom) into a standard space by the HCP preprocessing pipeline (16,17). One example of a color-coded DTI map is displayed in Figure 1.

Image Processing

Diffusion tensor (DT) estimation and diffusion scalar map calculations were performed in *3D Slicer* (version 4.8, Boston, MA) (18) in the dMRI extension (19). From the estimated DT, the principal eigenvector (main direction of diffusion) was extracted by the *DTIProcess* (C. Goodlett, version 2.0, Universities of Utah and North Carolina). Also derived from the DT, diffusion scalar maps were calculated for fractional anisotropy (FA), mean diffusivity (MD), and Mode.

Localization of Anatomical Structures and Labeling

The (50 μm isotropic) high-resolution anatomic brainstem reference MRI was manually registered (affine registration) to each HCP DTI image in *3D Slicer*. Landmarks (Fig. 1) included clearly visible structures, such as the pontine midline, the cochleovestibular nerves of both sides, the floor of the 4th ventricle, as well as the inferior and medial cerebellar penduncles (ICP, MCP). This allowed for a combined visualisation of the HCP DTI and the anatomical reference (Fig. 2), and the determination of the location of the CN and its demarcating structure (ICP caudal, medial, and rostral to the CN). Two voxels were labeled in each structure, namely the CN (Fig. 2), the ICP caudally, medially and rostrally to the CN. The location of the measurements in the brainstem is shown in Figure 3.

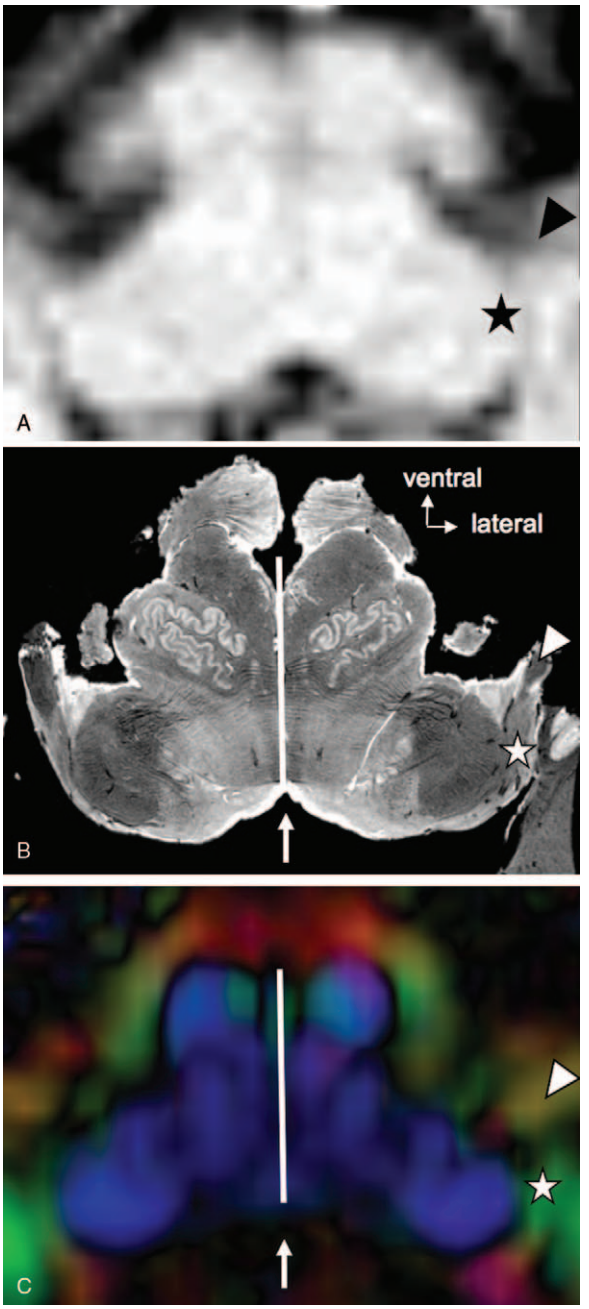

FIG. 1. Comparison of MRI and DTI brainstem images. *A*, Typical axial section of an anatomic T1-weighted MRI of the human brainstem at the level of the cochlear nucleus (CN, black *star*) at a resolution of 1.05 mm^3. The cochleovestibular nerve (cranial nerve VIII) is barely visible (black *arrow*), but the CN boundaries are not visible. *B*, High-resolution anatomic MRI image (resolution 50 μm). The cranial nerve VIII (white *arrow*) and CN boundaries (white *star*) are now clearly distinct. *C*, Diffusion tensor image (DTI, resolution 1.05 mm^3) from the Human Connectome Project. The structures are now resolved by fiber orientations, which are color coded: green stands for ventral-dorsal, red for lateral-lateral, blue for caudal-rostral fiber orientation. Yellow represents fiber orientations between green and red. Landmarks for the combination of the anatomic MRI (*B*) and DTI image (*C*) were the cranial nerve VIII (white *arrowhead*), the pontine midline (white *bar*), and the floor of the 4th ventricle (white *arrow*), among others.

Definition of FA, MD, Mode, and Eigenvectors

In DTI images, diffusion of free water molecules is represented by a three-dimensional diffusion tensor (DT) and is based on the assumption of a Gaussian distribution of water diffusion (7). The DT can be described by three orthogonal eigenvectors (V1, V2, V3) and their eigenvalues that indicate the magnitude of diffusion in each of the three directions. The eigenvector with the highest eigenvalue (V1) lies in the direction of major principal diffusion and is termed the principal eigenvector for this purpose. The eigenvalues are expressed as λ1, λ2, λ3, whereas λ1 refers to the largest eigenvalue and λ3 to the smallest one. From these eigenvalues, diffusion scalar values are derived that reflect the shape of the DT. They are useful measures to assess the degree of anisotropy, i.e., the degree of restricted diffusion in the tissue of interest. The diffusion scalar values used here are fractional anisotropy (FA), mean diffusivity (MD), and mode of anisotropy (Mode). MD reflects the mean of the three eigenvalues λ1, λ2, λ3. FA and Mode are orthogonal measures (20). FA varies between 0 (no diffusion restriction, e.g., free water) and 1 (diffusion only in one direction). Mode reflects the flatness of the DT and varies between −1 (pancake shape of the DT, lamellar diffusion) and 1 (tubular diffusion).

Assessment of FA, MD, Mode, and Principal Eigenvectors

Our strategy was to combine data for structures from the right and left sides for final reporting, which has two advantages: 1) there is better readability of complex data and 2) smaller vectors with less diffusion are weighted less in the resulting vector than vectors with a larger magnitude. To do this, the mean FA, MD, and Mode values of the voxels for each structure were read out by the module *''Label Statistics''* in *3D Slicer* for the left and for the right sides. Components (x, y, z) of the principal eigenvectors (V1) were read out directly from the corresponding map for each label. (x, y, z) are the components of the left, dorsal, and rostral axes of the images, respectively. Vectors from the right side were flipped to the left across the sagittal plane to give one value for the CN and its demarcating structures. The mean of the vectors was then obtained by adding all vectors for each structure and dividing them by their number. For a quantitative analysis, the angles of the principal eigenvector (V1) to the sagittal and axial planes of the image were calculated and termed azimuth (α) and declination (δ), respectively (Fig. 4). The azimuth represents the angle in degrees between the run (x,y) of the principal eigenvector (V1) and the sagittal plane, according to the formula $\alpha = \frac{180}{\pi} * \tan^{-1}\frac{x}{y}$. The declination determines the incline of the principal eigenvector (V1) in degrees from the axial plane, as expressed in the formula $\delta = \frac{180}{\pi} * \tan^{-1}\frac{z}{\sqrt{x^2+y^2}} * \frac{-y}{|y|}$.

Statistical Analysis

Paired *t test* was used to analyze the significance of comparisons between measures from anatomical structures as appropriate. A two-sided p value of <0.001 was considered significant. No correction for multiple testing was applied. No data was excluded. Statistical analyses were performed using SPSS (version 23, IBM Corp, Armonk, NY) and R (Vienna, Austria, Version 2018-06-06, vector analysis).

RESULTS

Subjects

One hundred subjects with a total of 200 CNs were analyzed. Age range was 22 to 35 years. There was a

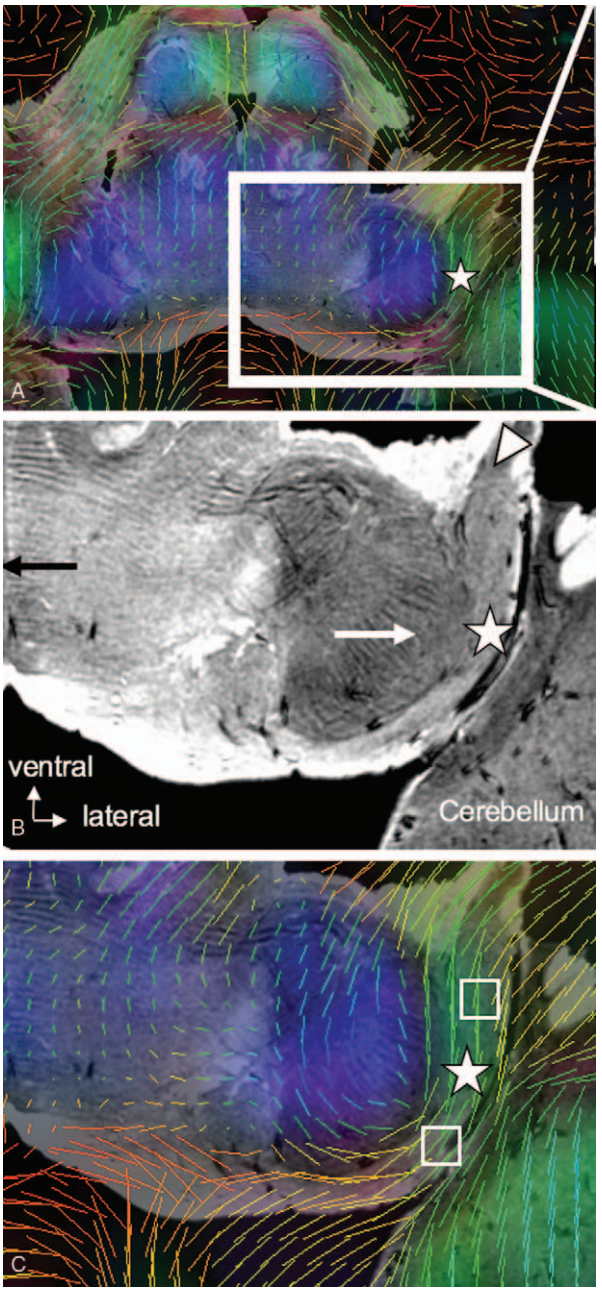

FIG. 2. MRI and DTI brainstem images. *A*, Combined diffusion tensor image (DTI) and anatomic high-resolution (50 μm) MRI image based on landmarks demonstrated in Figure 1. The principal eigenvectors showing the direction of diffusion are depicted as lines using the color-coding of Figure 1C. CN is indicated by the white star. *B*, Magnification of a portion of the anatomic high resolution MRI image: CN (white *star*) and the medially lying inferior cerebellar peduncle (ICP, white *arrow*). Ventro-laterally the cranial nerve VIII (white *arrowhead*) enters the CN. Among others, the cranial nerve VIII and the midline (black *arrow*) served as clear landmarks for combination (coregistration) of the high-resolution anatomical scan with the DTI images. *C*, Magnification of a portion of A (combined image) of one subject. Measurements were taken from two voxels within the CN (white *squares*).

slight female predominance of 59%. Median speech-in-noise threshold was 4.6 dB ± 1.34 dB (measured by the NIH Toolbox Words-in-Noise audiometric testing (11)).

Principal Eigenvectors

The angles are reported as if seen from the 4th ventricle (definition of directions visualized in Fig. 4). In the CN, the principal diffusion occurred in a dorsal-ventral orientation deviating to some degree laterally ($\alpha = -17.7° \pm 38.86°$) and was slightly tilted caudally from where the cochlear nerve entered the nucleus toward the dorsal part of the nucleus ($\delta = 9.48° \pm 37.76°$, see Fig. 3, green *arrows*). This was significantly different from the fiber orientation in the ICP medial to the CN, where fibers ascended mainly along the caudal-rostral axis ($\alpha = 47.35° \pm 45.82°$, $\delta = -79.55° \pm 11.89°$, both $p < 0.001$, see Fig. 3, blue *arrows*). This was also true for the fibers in the ICP that composed the rostral and caudal margins of the CN. These ICP fibers were also significantly different from the CN fiber orientation (rostral margin: $\alpha = 18.5° \pm 38.84°$, $\delta = -78.1° \pm 21.79°$, both $p < 0.001$, caudal margin: $\alpha = -59.6° \pm 33.01°$, $\delta = 70.06° \pm 23.04°$, both $p < 0.001$).

Fractional Anisotropy (FA), Mean Diffusivity (MD), and Mode of Anisotropy (Mode)

Scalar values are reported for both sides together in Table 1. FA was significantly lower in the CN than in the ICP medial to it and in the ICP that formed the rostral margin of the CN (both $p < 0.001$). MD was significantly higher and Mode significantly lower in the CN compared with the ICP medial to it and in the ICP that formed the rostral margin (both $p < 0.001$). The lower Mode in the CN is indicatory of a more lamellar structure in the CN (Fig. 5). An additional comparison of the left and right CN revealed a significantly higher FA (0.47 ± 0.11 vs. 0.41 ± 0.11, $p < 0.001$) and higher MD ($0.74 \pm 0.77 \times 10^{-3}$ vs. $0.52 \pm 0.10 \times 10^{-3}$, $p = 0.005$) on the right side. Mode did not differ between the sides (right 0.59 ± 0.36 vs. left 0.63 ± 0.34, $p = 0.38$).

DISCUSSION

Key Results

This study shows that the principal fiber orientation in human CN follows a ventral-dorsal direction, as opposed to the caudal-rostral direction of the adjacent ICP. The fibers of the cochlear nerve descend slightly caudally after they enter the CN and project dorsally. We also demonstrate that FA and Mode are lower in the CN compared with its surroundings. Based on these findings and in contrast to conventional MRI sequences, the CN can be distinguished by DTI and potentially used for surgical planning and patient-specific ABI design.

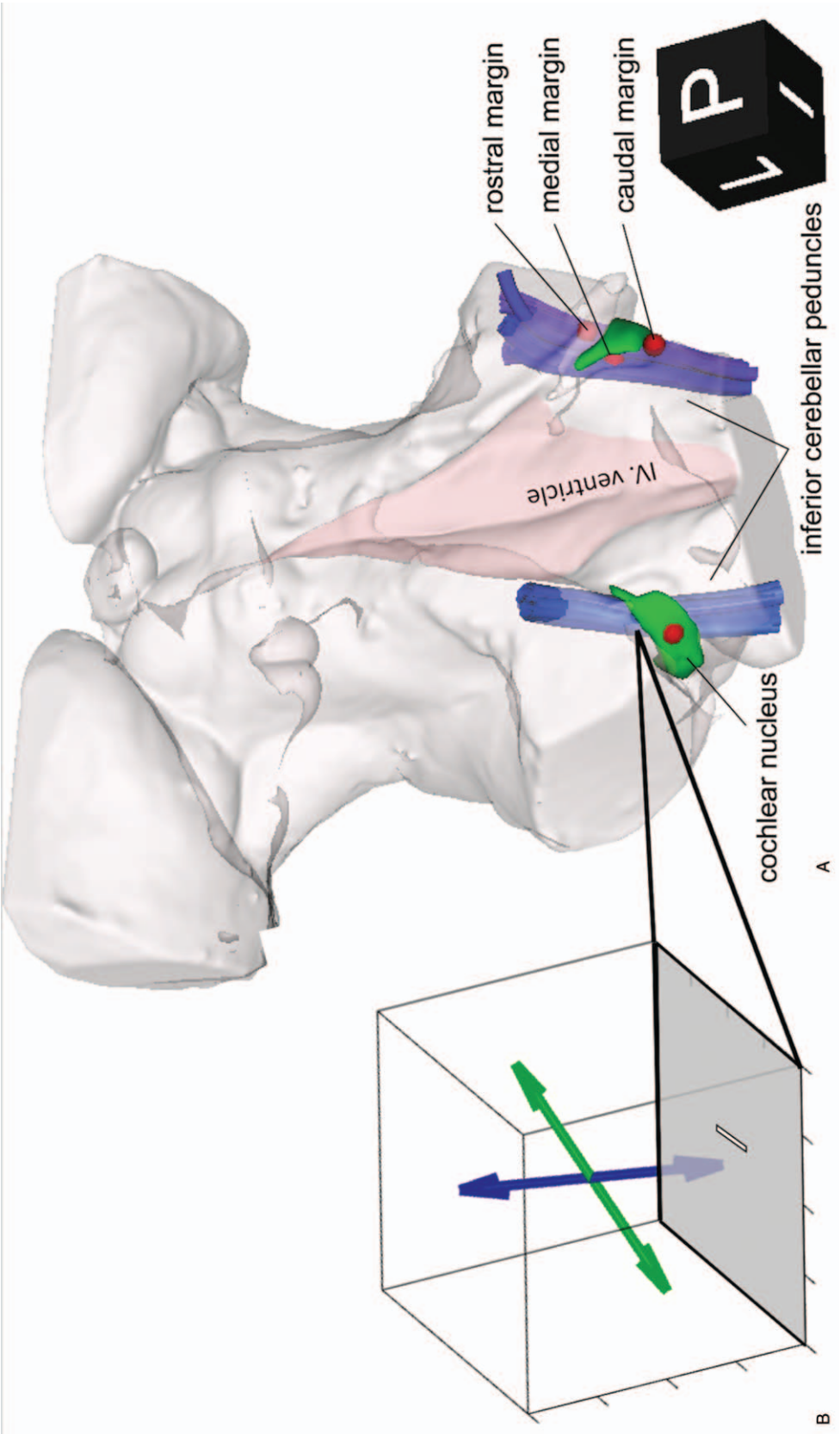

FIG. 3. *A*, Three-dimensional (3D) reconstruction of a human brainstem between the ponto-medullary junction and the thalamus. Colors mentioned in the following are as displayed in the online color version of the article. Highlighted are the CN (green) and the ICP (blue). The red dots represent the location of the different measurements for this study (caudal. medial, rostral margin of the CN with the ICP). The structures are visualized only on one side here. However, all structures were measured on both sides. *B*, Mean vectors in the box of the fiber orientation in the CN (dorsal-ventral, green) and the medial ICP (caudal-rostral, blue) using the angle of rotation of the 3D reconstruction of the brainstem. P: posterior (dorsal), I: Inferior (caudal), L: left.

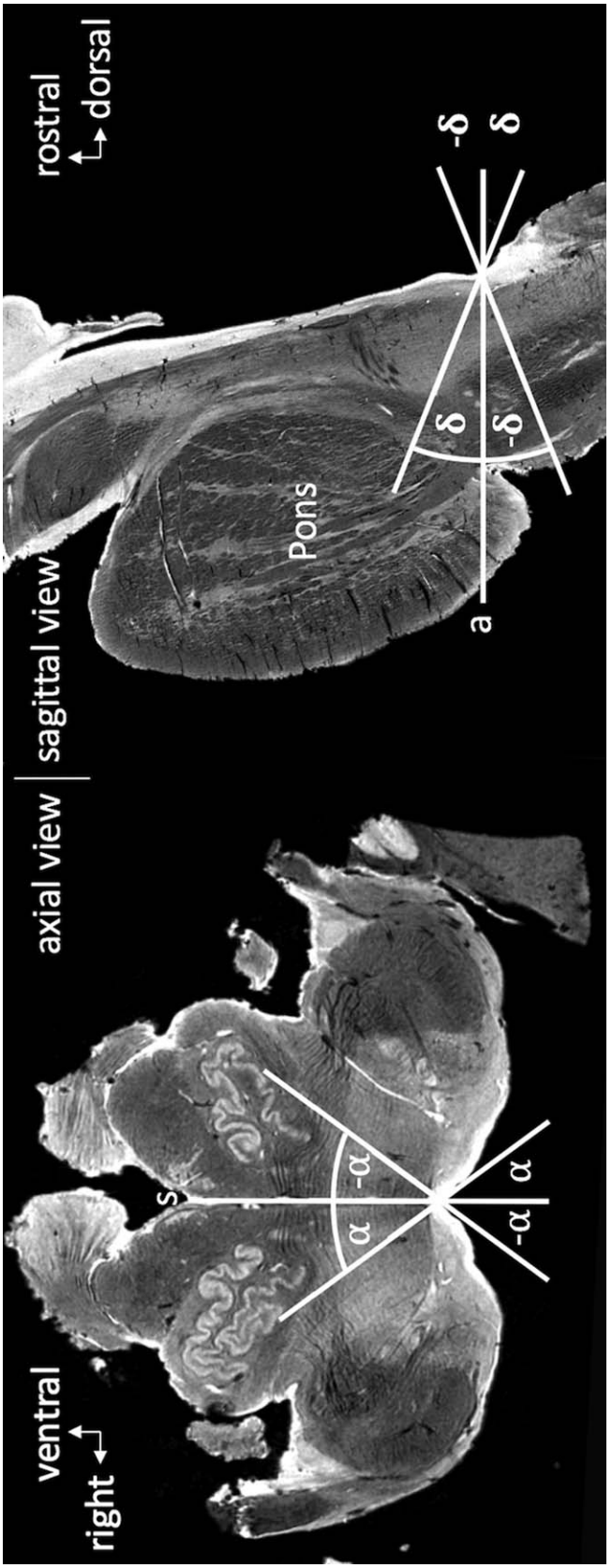

FIG. 4. High-resolution anatomic MRI and definition of vectors in the brainstem. The mean principal eigenvectors (V1) of the measured structures are converted into azimuth (α) and declination (δ). Azimuth (α) indicates the deviation of V1 from the sagittal plane (s). Declination (δ) is determined by the inclination of V1 from the axial plane (a). Positive values of α represent right-ventrally or left-dorsally pointed principal eigenvectors. Positive values for δ reflect ventral-rostrally or dorsal-caudally inclined principal eigenvectors.

TABLE 1. *Diffusion scalar values*

	FA	MD	Mode
CN	0.44 ± 0.09	0.63 ± 0.38	0.61 ± 0.27
ICP caudal margin	$0.47^{b} \pm 0.11$	0.71 ± 0.55	0.67 ± 0.26
ICP medial margin	$0.64^{a} \pm 0.08$	$0.55^{a} \pm 0.35$	$0.79^{a} \pm 0.20$
ICP rostral margin	$0.66^{a} \pm 0.08$	$0.47^{a} \pm 0.05$	$0.74^{a} \pm 0.23$

[a] Significantly different from CN value ([a] $p < 0.001$, [b] $p = 0.0138$).

CN indicates cochlear nucleus; FA, fractional anisotropy; ICP, inferior cerebellar peduncle; MD, mean diffusivity (expressed as $MD \times 1/10^{-3}$).

DTI and Histology

Our DTI findings from 100 volunteers are consistent with previous histologic descriptions. The cochleovestibular nerve enters the brainstem at the pontomedullary junction. In humans, rostral fibers of the cochlear nerve travel rostrally into the anterior ventral CN (AVCN). Caudal fibers travel through the posterior ventral cochlear nucleus (PVCN) into the dorsal CN (DCN) (21). The resulting main fiber orientation thus runs from ventro-rostral to dorsocaudal (Fig. 3, green *arrows*). The adjacent ICP runs almost orthogonally to the fibers of the CN and connects the spinal cord, the medulla, and the vestibular nuclei with the cerebellum in a mainly caudal-rostral direction (Fig. 3, blue *arrows*) (22). Both the anterior-posterior fiber orientation of the CN and the caudal-rostral orientation of the ICP are reproduced by DTI in our study (21).

The extracted diffusion scalar values FA and Mode also correspond to what is known histologically about CN anatomy. The FA in the CN was lower than in its adjacent structures, meaning that diffusion was less unidirectional in the nucleus compared with the ICP. This is in line with other measurements that showed lower FA in nuclei compared with tracts (23). In general, this is explained by the high cellularity and netlike interconnections in a brainstem nucleus that result in less unidirectional diffusion. The CN also showed a lower Mode than the ICP medially and rostrally, signifying that the diffusion was more lamellar (pancake shaped) than tubular (cigar shaped). This lamellar structure can be appreciated in the (50 μm) high-resolution anatomical scans used for this study (Fig. 5) and corresponds to known human histology showing that the primary fibers from the vestibulocochlear nerve lie in parallel to the surface and have an increasing lamellar organization toward the DCN (21,24,25). There was no significant difference between CN and the ICP caudally regarding MD and Mode. This might be due to the fact that the inferior margin lies at the outer surface of the brainstem and has similar lamellar properties.

Functional Considerations

In summary, DTI images can enable localization of the CN preoperatively. The resolution needed ($1\,mm^3$) can be achieved on modern MRI/DTI scanners. This is clinically relevant because functional outcomes depend on the accurate positioning of the ABI array, as previously shown by our group (6). Intraoperative placement of the ABI is challenging because the CN cannot be directly visualized in the lateral recess of the 4th ventricle (Fig. 6). As a result, audiologic outcomes for ABI users are variable with most subjects experiencing sound awareness (that aids in lipreading) but only a few having some speech recognition (2).

Traditionally, the ABI is placed along the axis of the lower cranial nerves (Fig. 6, black *arrow*). Based on our findings, *an insertion vector with the array directed more caudally* (Fig. 6, white *arrow*) would better correspond to the main fiber axis of the CN. DTI is an imaging modality that allows patient-specific assessment of the CN and highlights a possible role of surgical navigation to improve the accuracy of ABI placement.

Interestingly, we found a higher FA in the right CN compared with the left side. This might be an expression of a higher level of fiber organization in the CN on this side, clinically known as right ear advantage. This effect is known in single-sided deafness patients and describes the fact that patients who hear only on the right side perform better in speech hearing tests than patients who hear on the left side only (26). The effect was traditionally thought to be due to cortical processing mechanisms that are asymmetric between the left and right hemispheres. Our finding could indicate that this asymmetry is present on a subcortical level already. This finding also emphasizes the utility of DTI in the assessment of the central auditory pathway (27).

Limitations

There are several limitations of this study. It is possible that partial volume effects influence FA measurements in the CN. Measurements from a voxel covering mostly the CN, but also a small portion of cerebrospinal fluid, for example, would show an artificially lower FA compared with the ICP parts that are surrounded by neuronal tissue. The direction of the principal eigenvectors is not affected by these border issues. Since the primary score finally reported from HCP regarding PTA in this normal-hearing, young cohort is rather generic, we could not control for differences in interaural hearing thresholds. This could affect the observed interaural FA differences in the CN. Some variations of our results are possibly due to the registration process of the anatomic

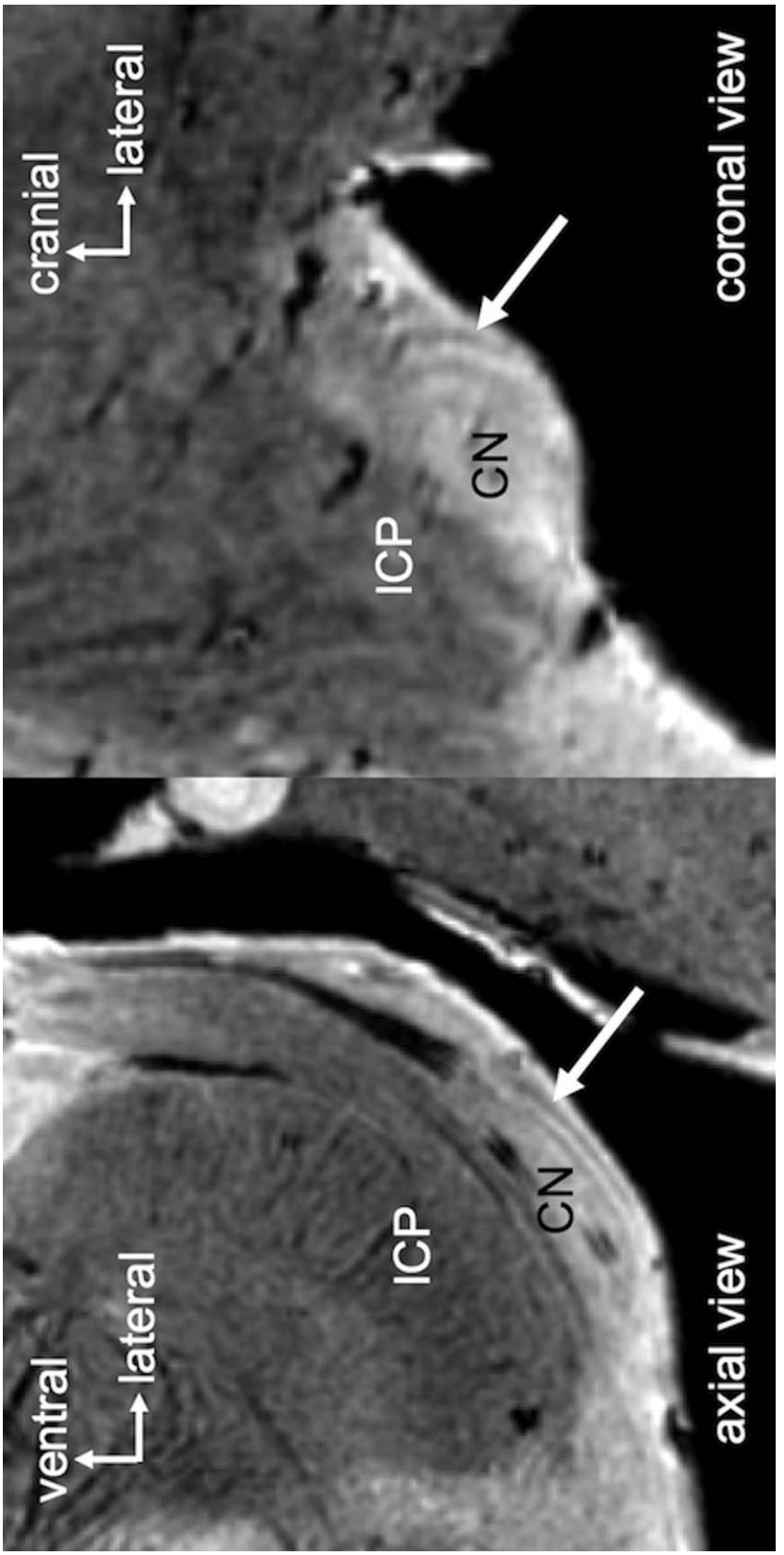

FIG. 5. High-resolution anatomical scans showing CN with adjacent ICP. White *arrows* point to locations in the CN where a lamellar structure can be appreciated.

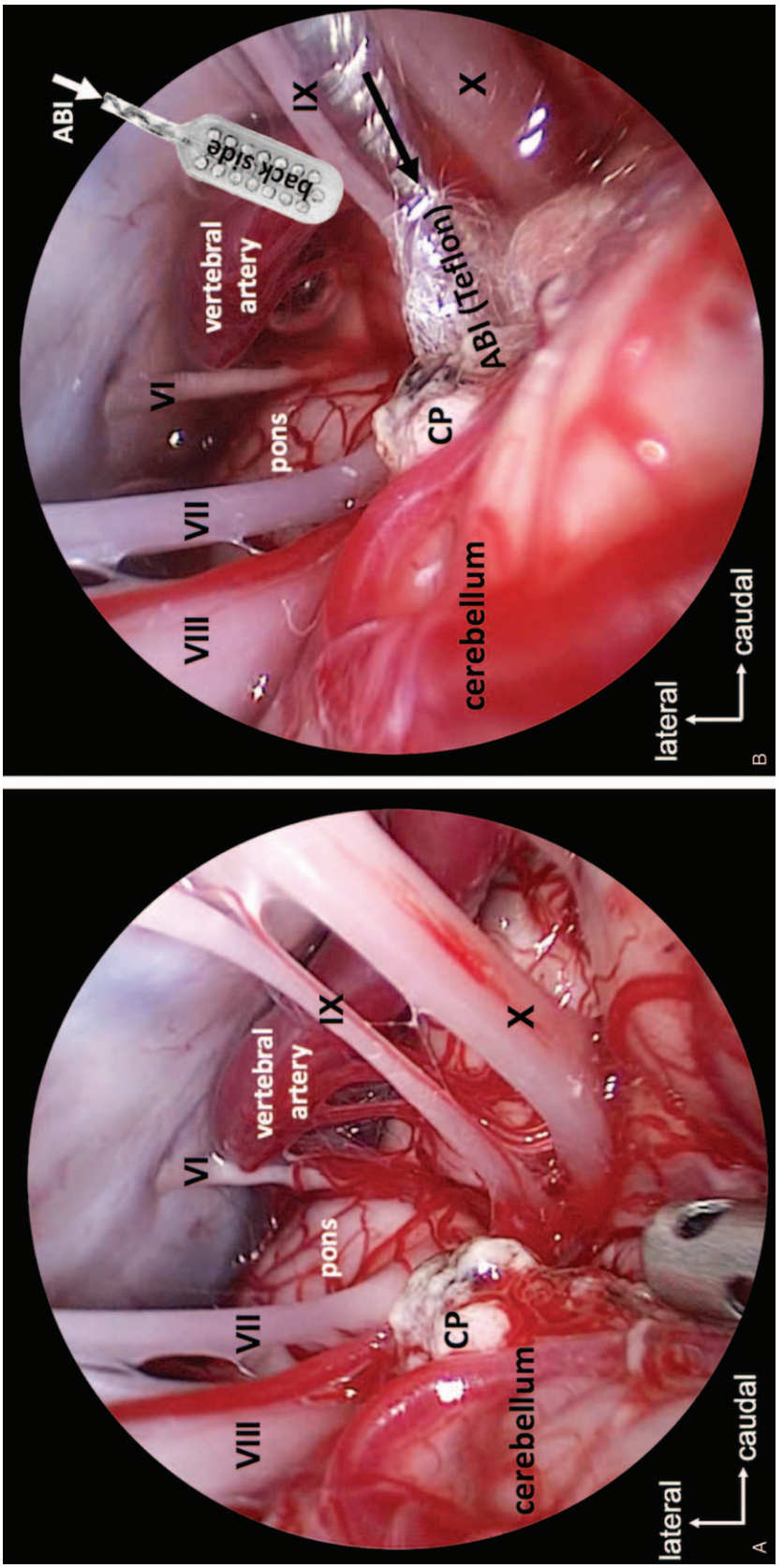

FIG. 6. Retrosigmoid craniotomy, right ear. *A*, Surgical view of the posterior fossa with a 0° 4 mm diameter rigid endoscope. The roots of cranial nerves IX and X and the choroid plexus (CP) are visualized as anatomical landmarks. In (*B*) the ABI electrode array (black *arrow*) is inserted into the lateral recess of the 4th ventricle (with electrode contacts facing AWAY from the surgeon) and stabilized with Teflon felt (shown) and autologous muscle (not shown). The CN is not visualized directly because of the overlying cerebellum. Based on our imaging findings, a modified surgical approach with the ABI array oriented more *caudally* along the main axis of the fibers of the dorsal CN would be possible (white *arrow*). VI indicates abducens nerve; VII, facial nerve; VIII, vestibular nerve.

high-resolution image to the lower resolution HCP DTI images. We tried to reduce this variation to a minimum by using clearly predefined landmarks and by manually registering each image separately. The variation of our results is in the order of magnitude of the naturally occurring variation of diffusion scalar values between subjects (28).

CONCLUSION

DTI enables the direct visualization of CN location and its neuronal substructure. This visualization is made possible because the fibers in the CN and adjacent ICP run in clearly distinct directions. These findings have implications for the direct visualization of the CN in the clinical context of ABI implantation. They suggest that an ABI array insertion vector directed more caudally would better correspond to the main fiber axis of CN. Future studies will focus on applying our approach to patients with brainstem distortion secondary to growth of large vestibular schwannoma.

Acknowledgments: Prof. G. Allan Johnson, Department of Radiology, Duke University, Durham, NC, USA.

REFERENCES

1. Ramsden RT, Freeman SRM, Lloyd SKW, et al. Auditory brainstem implantation in neurofibromatosis type 2. *Otol Neurotol* 2016;7:1267–74.
2. Colletti V, Shannon R, Carner M, Veronese S, Colletti L. Outcomes in nontumor adults fitted with the auditory brainstem implant: 10 years' experience. *Otol Neurotol* 2009;30:614–8.
3. Abe H, Rhoton AL. Microsurgical anatomy of the cochlear nuclei. *Neurosurgery* 2006;58:728–38.
4. Quester R, Schröder R. Topographic anatomy of the cochlear nuclear region at the floor of the fourth ventricle in humans. *J Neurosurg* 1999;91:466–76.
5. Rosahl SK, Rosahl S. No easy target: anatomic constraints of electrodes interfacing the human cochlear nucleus. *Neurosurgery* 2013;72:. 58–64.
6. Barber SR, Kozin ED, Remenschneider AK, et al. Auditory brainstem implant array position varies widely among adult and pediatric patients and is associated with perception. *Ear Hear* 2017;38:e343–51.
7. O'Donnell L, Westin C-F. An introduction to diffusion tensor image analysis. *Neurosurg Clin N Am* 2012;22:1–23.
8. Reiman M, Parkkola R, Johansson R, et al. Diffusion tensor imaging of the inferior colliculus and brainstem auditory-evoked potentials in preterm infants. *Pediatr Radiol* 2009;39:804–9.
9. Dieterich M, Kirsch V, Brandt T. Right-sided dominance of the bilateral vestibular system in the upper brainstem and thalamus. *J Neurol* 2017;264:55–62.
10. Naidich TP, Duvernoy HM, Delman BN, Sorensen GA, Kollias SS, Haacke EM. *Duvernoy's Atlas of the Human Brain Stem and Cerebellum*. Vienna, Wien, NewYork: Springer; 2009.
11. Zecker SG, Hoffman HJ, Frisina R, et al. Audition assessment using the NIH Toolbox. *Neurology* 2013;80 (suppl 3):S45–8.
12. Calabrese E, Hickey P, Hulette C, et al. Postmortem diffusion MRI of the human brainstem and thalamus for deep brain stimulator electrode localization. *Hum Brain Mapp* 2015;36:3167–78.
13. Sotiropoulos SN, Moeller S, Jbabdi S, et al. Effects of image reconstruction on fiber orientation mapping from multichannel diffusion MRI: Reducing the noise floor using SENSE. *Magn Reson Med* 2013;70:1682–9.
14. Andersson JLR, Skare S, Ashburner J. How to correct susceptibility distortions in spin-echo echo-planar images: Application to diffusion tensor imaging. *Neuroimage* 2003;20:870–88.
15. Andersson JLR, Sotiropoulos SN. Non-parametric representation and prediction of single- and multi-shell diffusion-weighted MRI data using Gaussian processes. *Neuroimage* 2015;122: 166–76.
16. Glasser MF, Sotiropoulos SN, Wilson JA, et al. The minimal preprocessing pipelines for the Human Connectome Project. Mandal PK, ed. *Neuroimage* 2013;80:105–24.
17. Mandal PK, Mahajan R, Dinov ID. Structural brain atlases: Design, rationale, and applications in normal and pathological cohorts. Mandal PK, ed. *J Alzheimer's Dis* 2012;31:S169–88.
18. Fedorov A, Beichel R, Kalphaty-Cramer J, et al. 3D slicers as an image computing platform for thw quantitative imaging network. *Magn Reson Imaging* 2012;30:1323–41.
19. Norton I, Essayed WI, Zhang F, et al. SlicerDMRI: Open source diffusion MRI software for brain cancer research. *Cancer Res* 2017;77:e101–3.
20. Ennis DB, Kindlmann G. Orthogonal tensor invariants and the analysis of diffusion tensor magnetic resonance images. *Magn Reson Med* 2006;55:136–46.
21. Amunts K, Morosan P, Hilbig H, Zilles K. *Auditory System*. 3rd ed. Chapter 36 in The Human Nervous System. New York, NY: Elsevier, 2012.
22. Parent A. *Carpenter's Human Neuroanatomy*. 9th ed. Baltimore, MD: Wolters Kluwer, 1995.
23. Pal D, Trivedi R, Saksena S, et al. Quantification of age- and gender-related changes in diffusion tensor imaging indices in deep grey matter of the normal human brain. *J Clin Neurosci* 2011;18: 193–6.
24. Büttner-Ennever JA, Horn AKE. *Olszewski and Baxter's Cytoarchitecture of the Human Brainstem*. Munich, Germany: S. Karger AG, 2014.
25. Lorente de Nò R. *The Primary Acoustic Nuclei*. New York, NY: Raven Press, 1981.
26. Wettstein VG, Probst R. Right ear advantage of speech audiometry in single-sided deafness. *Otol Neurotol* 2018;39:417–21.
27. Tarabichi O, Kozin ED, Kanumuri VV, et al. Diffusion tensor imaging of central auditory pathways in patients with sensorineural hearing loss: A systematic review. *Otolaryngol Head Neck Surg* 2018;158:432–42.
28. Lawrenz M, Brassen S, Finsterbusch J. Microscopic diffusion anisotropy in the human brain: Reproducibility, normal values, and comparison with the fractional anisotropy. *Neuroimage* 2015;109:283–97.